



HAL
open science

Nitrogen quantification and tracking during high temperature oxidation in air of titanium using ^{15}N isotopic labelling

Virgil Optasanu, Pascal Berger, M. C. Marco de Lucas, M. Khan Rayhan, F. Herbst, N. Geoffroy, O. Heintz, Igor Bezverkhyy, S. Chevalier, T. Montesin, et al.

► To cite this version:

Virgil Optasanu, Pascal Berger, M. C. Marco de Lucas, M. Khan Rayhan, F. Herbst, et al.. Nitrogen quantification and tracking during high temperature oxidation in air of titanium using ^{15}N isotopic labelling. *Corrosion Science*, 2023, 216, pp.111072. 10.1016/j.corsci.2023.111072 . hal-04012282

HAL Id: hal-04012282

<https://hal.science/hal-04012282>

Submitted on 2 Mar 2023

HAL is a multi-disciplinary open access archive for the deposit and dissemination of scientific research documents, whether they are published or not. The documents may come from teaching and research institutions in France or abroad, or from public or private research centers.

L'archive ouverte pluridisciplinaire **HAL**, est destinée au dépôt et à la diffusion de documents scientifiques de niveau recherche, publiés ou non, émanant des établissements d'enseignement et de recherche français ou étrangers, des laboratoires publics ou privés.

Find the official publication here : <https://doi.org/10.1016/j.corsci.2023.111072>

Nitrogen quantification and tracking during high temperature oxidation in air of Titanium using ^{15}N isotopic labelling

V. Optasanu^{a,*}, P. Berger^b, M. C. Marco de Lucas^a, M. Khan Rayhan^a, F. Herbst^a, N. Geoffroy^a, O. Heintz^a, I. Bezverkhyy^a, S. Chevalier^a, T. Montesin^a, L. Lavissee^a

^a ICB UMR 6303 CNRS, Université de Bourgogne, 9 av. Alain Savary, BP 47870, F-21078 Dijon Cedex, France

^b Université Paris-Saclay, CEA, CNRS, NIMBE, 91191 Gif-sur-Yvette, France

virgil.optasanu@u-bourgogne.fr; pascal.berger@cea.fr; mrayhan13@yahoo.com;
frederic.herbst@u-bourgogne.fr; nicolas.geoffroy@u-bourgogne.fr; delucas@u-bourgogne.fr;
olivier.heintz@u-bourgogne.fr; igor.bezverkhyy@u-bourgogne.fr;
sebastien.chevalier@u-bourgogne.fr; tony.montesin@u-bourgogne.fr; luc.lavissee@u-bourgogne.fr

Abstract

Isotopic labelling was used to track the diffusion of nitrogen during the oxidation of Titanium in air at 700°C. Alternate exposure in $^{15}\text{N}_2$ -labelled air and regular air was used. The nitrogen is mainly located at the oxide/metal interface and forms essentially a nitride phase close to Ti_2N . Each nitrogen isotope was quantified by Nuclear Reaction Analysis. Nitrogen quantity doubles between 5 and 20 h, which represents 16 % respectively 12.5 %, of the total mass gains. The nitrogen is partially renewed by both inward and outward diffusion during the oxidation. A model for nitrides migration is proposed.

Keywords

Titanium, oxidation, N_2/O_2 diffusion, nitrides, nuclear reaction analysis

1. Introduction

Titanium and its alloys are increasingly used in industrial applications thanks to their interesting mechanical properties and to their good resistance to corrosion. However, the high temperature use of titanium and their alloys are limited by oxidation, which is mainly based on an anionic mechanism at temperatures lower than 800°C [1]. The atmospheric oxygen diffuses through the oxide scale. A fraction of this oxygen contributes to forming new oxides at the interface oxide/metal and the balance of it continues to diffuse within the metal as interstitial solid solution. Thus, the oxide layer is protective if it is dense and unfractured. The oxygen solid solution, sometimes called alpha-case is hard and brittle. Its oxygen-content can go up to 33 at. % [1].

Many studies point out the role of the nitrogen in the oxidation of titanium and alloys in air. Thus, Chaze and Coddet [2], observed that the presence of nitrogen slowed down the rate of oxidation compared to oxidation under pure oxygen at equivalent partial pressure. They also remarked that the adhesion of the oxide layers formed under air atmosphere is improved compared to oxides obtained under pure oxygen. Other authors pointed out more recently the role of the atmospheric nitrogen during the oxidation in air and showed the nitrogen is located at the interface oxide/metal of commercial pure titanium [3–7], near-alpha Ti alloys [7–9] or beta meta-stable Ti alloy [6].

Kanjer et al. [3–5] and Lavisse et al. [6,7] showed that the quantity of nitrogen is dependent on the mechanical treatment that the metal underwent prior to oxidation in air. Thus, mechanical treatments like shot-peening and laser-shock peening showed beneficial results on the high temperature oxidation resistance of titanium in air and were associated with bigger quantities of nitrogen observed at the oxide/metal interface. Dupressoire et al. [8] showed that the oxidation rate of Ti6242 alloy is substantially lower in synthetic air than in a mixture of 80% Ar - 20% O₂. Kitashima et al. [11] showed the presence of nitrogen and highlighted the role of nitrogen in the recrystallization of some titanium grains at the oxide/metal interface of a near-alpha titanium alloy oxidized at 750 °C in air. They suggested that the presence of nitrides plays a role in the recrystallization process and showed that the recrystallized grains contain less oxygen than the non-crystallized grains. Abdallah et al. [9] observed the presence of Ti₂N, TiN and TiO_xN_y phases at the interface between oxide and metal in Ti6242 alloy oxidized for 1000 h at 650 °C in air. They showed that the nitrides are not present in a continuous layer.

While the presence of nitrogen at the oxide/metal interface from the first hours of exposure at high temperatures is well proven now, the kinetic of insertion of the nitrogen is however still not investigated. Several questions are then worth to be studied:

- How much nitrogen is inserted during the oxidation?
- Does the quantity of inserted nitrogen vary as a function of the time?
- Is the nitrogen quantity renewed during the oxidation or is the quantity initially inserted trapped at the oxide/metal interface that travels with the interface?

In order to answer these questions, experiments of isotopic labelling with ¹⁵N-rich air were carried by oxidation tests led at 700 °C during relatively short durations: 5 h and 20 h. The kinetics of nitrogen insertion were revealed using two-stages oxidation using regular air (80% N₂, 20% O₂) and ¹⁵N-labelled air (80% ¹⁵N₂, 20% O₂). The switch between the two atmospheres (containing two different isotopes of nitrogen) during the oxidation permits to track the path of nitrogen and then reveals the mechanism of insertion of this element.

There are very few works in the literature using nitrogen isotopic labelling during oxidation of titanium and titanium alloys. Haanapel et al. [12] used two stages oxidation studies with ¹⁵N tracers to highlight the mechanisms of oxidation of Ti-Al based alloys. Carpenne et al. [13] studied laser nitridation of titanium under nitrogen atmosphere with ¹⁵N isotope. Göbel et al. [14] exploited isotopic tracers to study the oxidation of titanium and Ti-Nb alloy at 800°C under dry and humid air and used secondary neutral mass spectrometry to find the distribution of nitrogen and oxygen as a function of depth.

To our knowledge this is the first time when the tracking of nitrogen by isotopic labelling is used for titanium to quantify the nitrogen mass gain on samples oxidized in air at 700°C combined with the Nuclear Reaction Analysis for accurate quantification.

2. Materials and Methods

2.1. Material and sample preparation

Commercially pure Titanium (1 mm thick cold-rolled and annealed plates, purity 99,6%, grade 1, Goodfellow Supplier) was cut in samples of 10 x 10 mm². The cutting edges were slightly rounded in order to avoid geometrical singularities that could provoke partial

delamination of the oxide. The samples were polished up to P1200 grit, washed, cleaned in ethanol and distilled water, dried, measured and weighted.

The samples were oxidized at 700 °C in a quartz tube and a tubular furnace for two durations and with various controlled atmospheres, as presented in Table 1. The pressure of the atmosphere was 1 bar. We will refer to each sample using the name declared in the first column of this table. The periods of exposure were chosen in order to produce oxides of about 1 µm thick after 5 h of exposure and about the double after 20 h of exposure, as the oxide thickness goes approximately with the square root of the time at this temperature.

After the oxidation the samples were weighted in order to determine the mass gain. For the short oxidation durations studied here, the thickness of the oxide scales is small (few microns). This allowed us to investigate the whole thickness of the scale, up to the metal substrate, by XRD, nuclear reaction analysis (NRA), and secondary ions mass spectrometry (SIMS).

Table 1. Ti samples identification and corresponding oxidation treatments.

Sample	Oxidation step 1		Oxidation step 2		Total exposure
	Time (h)	Atmosphere	Time (h)	Atmosphere	Time (h)
S1	5	N ₂ +O ₂	-		5
S2	5	¹⁵ N ₂ +O ₂	-		5
S3	5	¹⁵ N ₂ +O ₂	15	N ₂ +O ₂	20

In the followings, for readability reasons, we will designate the mix 80% N₂+ 20% O₂ as regular synthetic air, and the mix 80% ¹⁵N₂+ 20% O₂ as ¹⁵N-labelled air.

The oxidized samples were crosscut, coated with very thin Au layer by PVD technique in order to enhance the conductivity of the oxidized surface, then electrolytically coated with a thick Cu layer to prevent or limit the oxide delamination during the polishing process. Then the samples were resin embedded and mirror-polished up to 30 nm colloidal silica suspension.

2.2. Experimental device for isotopic labeling and high temperature oxidation

The experimental device used for isotopic labelling is presented in Figure 1. The isotopic labelling was made at 700°C by interrupted oxidation with dry synthetic air and/or ¹⁵N-labelled air (Euriso-top supplier, ¹⁵N purity 99.0 %) In order to reuse the onerous ¹⁵N-labelled air, a cryogenic trap with zeolite was used. The schematic of the isotopic labelling setup is presented in Figure 1. A thermocouple is mounted close to the sample (not represented on the schematic) in order to precisely control the temperature. For the sample S3 the oxidation is made for the first 5 h under ¹⁵N-labelled air followed by a rapid trapping of the oxidative atmosphere using the cryogenic unit made from zeolite and cooled down in liquid nitrogen. The trapping process is very rapid, in less than 1 min the pressure within the chamber drops below 5.10⁻⁵ mbar, which is the minimum pressure that can be measured by the vacuum gauge used here. Once the cryogenic reservoir isolated, the chamber is filled for the next 15 h of oxidation with regular synthetic air. Thus, the switch

in the atmosphere nature is sudden and the samples are kept at constant temperature during the gas change.

The furnace used here is mounted on bearings that allow it to be moved up and down in order to heat and cool down the sample in few minutes. These steps are important since the oxidation times are relatively short.

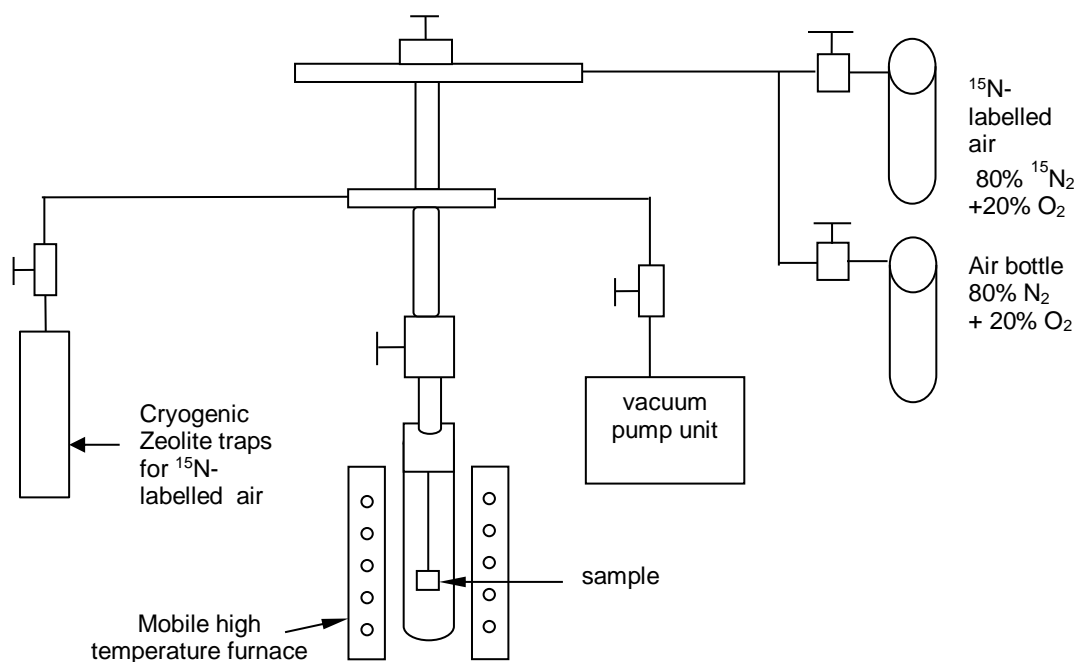


Figure 1. Experimental device for isotopic labelling during oxidation.

2.3. Characterization methods

The oxidized samples were analysed by XRD techniques in two different configurations: fix grazing incidence and Bragg-Brentano (theta-theta) mode. The grazing incidence diffraction patterns were made with grazing angles: 1° , 2° , 4° and 8° . The goniometer used in this study was Bruker D8-A25 Discover with $\text{Cu K}\alpha_{1,2}$ tube. The experimental diffraction patterns were fitted by Rietveld techniques using Topas V6 software in PV_TCHZ mode. A standard corundum sample SRM1976b was used to quantify the instrumental broadening. The XRD patterns recorded in theta - theta mode covered a range of 2θ scale from 20° to 80° .

Raman spectroscopy was used to investigate the non-metallic phases formed in the oxidized samples. Spectra were made at room temperature using a Renishaw inVia micro-Raman spectrometer in backscattering configuration. The spectra were recorded with a 532 nm wavelength laser as excitation source. The laser power was about 2.5 mW to avoid heating the sample.

The high-resolution scanning electron microscope images were taken using a Schottky field emission SEM JEOL JSM-7600F with LABE detector (Low Angle Backscattered Electron).

The EDS/WDS cartographies were recorded using JEOL JSM7600F SEM equipped with Oxford Instruments energy dispersive (EDS) SDD X-max 80 mm² and wavelength dispersive spectroscopy (WDS) INCA Wave 500 detectors.

The in-depth distribution of oxygen and nitrogen were also investigated by SIMS with NanoTOF II apparatus (ULVAC-PHI). TOF analyses are done using Bi₃²⁺ primary ions in 40x40 μm² area (30 keV). Cs⁺ ions in 200x200 μm² (2keV – 2nA) are used before analysis for sputtering sequences. Negative secondary ions are monitored, in particular ¹⁶O⁻, ¹²C¹⁴N⁻ and ¹²C¹⁵N⁻ for respectively oxygen and nitrogen elements.

The nitrogen isotopic composition and profile of the oxidized samples were investigated by Nuclear Reaction Analysis [15,16] performed at CEA Saclay (LEEL Laboratory of CNRS/CEA), France [17,18]. A 1.9 MeV deuteron (d⁺, deuterium ion) micro-beam (size 2.5 x 4 μm²) was directed perpendicularly to the samples surface and the emitted particles were detected backwards at 170° from the beam axis. The energy of the beam was chosen to be the highest deliverable by the accelerator for deuteron beams in order to maximize the cross-section (which is the probability to occur) of the nuclear reactions on ¹⁵N and ¹⁴N isotopes. At this energy, nuclear reactions with other light elements like ¹⁶O and ¹²C can also occur. They are used for calibration purposes. The NRA technique allows to quantify the concentration of all light elements present in the samples and to discriminate between their isotopes.

The Table 2 indicates the nuclear reactions we have considered to quantify the ¹⁴N and ¹⁵N profiles. Since the amount of energy released by a given nuclear reaction is a characteristic feature of it, the energy of the particles produced at the surface of the sample is a signature of the reaction. This energy can be calculated according to the beam conditions and confirmed by the measurement of known calibrated samples.

As both deuterons of the incident beam and particles produced by the nuclear reactions lose energy when travelling through solid matter. Then, any shift of the detected particle energy towards lower values (compared to the nominal value) indicates that the reactions occur deeper into the material. From the value of the shift and the knowledge of stopping power of the material one can calculate the thickness of the solid matter the particles have traversed. Hence, the depth at which the reactions occurred can be determined. So, the energy shift from the nominal value can be converted into a depth scale. The intensity profile of the signal depends on the concentration of the element at a given depth and to the related cross section (probability) of the reaction. Then, concentration depth profiles can be extracted from NRA spectra from the surface over depths of several μm, without any destructive preparation. The size of the scans was 200 x 200 μm², which covers several grains. Thus, the information obtained by this technique on the concentration or location of elements represents an average value over this area.

Table 2. Experimental conditions of the Nuclear Reaction Analysis used for this experiment and nuclear reactions used to reveal the nitrogen isotopes.

Beam energy	Nuclear reaction	Energy released by the reaction (keV)	Energy of the emitted α particle at the surface (keV)	Ref. for the cross-section of reactions
1.9 MeV	¹⁵ N(d,α ₀) ¹³ C	7687	6001	[19,20]
	¹⁴ N(d,α ₁) ¹² C	9136	6788	[19,21]

3. Results

3.1. Mass gain

The samples were weighted before and after the high temperature exposure in order to determine the overall mass gain per unit area. The results are given in Table 3. One can remark that the mass gains under regular air and ^{15}N -labelled air increase with the exposure time, as expected. The samples S1 and S2 present very similar mass gains, which confirm the fact that the two isotopes induce similar behaviours. The mass gain values obtained in the presented work during 5 and 20 h of oxidation are nearly those reported in previous works for pure titanium at 700 °C [5,7]. For short-time exposures, Kanjer et al. [5] found a nearly linear oxidation kinetics up to about 7 h, while the mass gain variation was close to parabolic kinetic law from 7 up to 40 h, which corresponds to a rate-limiting process given by the diffusion of oxygen through a dense and protective barrier.

Table 3. Measured mass gain per unit area of the samples after various expositions at 700°C.

Sample	oxidation duration (h)	Mass gain $\Delta m/S$ (mg/cm ²)
S1	5	0.251
S2	5	0.245
S3	20	0.689

3.2. Structure of oxide layers

3.2.1. Microscopic investigations

The microscopic images of the samples can be found in Figure 2. The oxide layers (grey, grainy layers on the top of the images) thicknesses are inhomogeneous with average values of $\sim 1 \mu\text{m}$, $\sim 1 \mu\text{m}$ and $\sim 3 \mu\text{m}$ for, S1, S2, and respectively S3 samples. The images show equiaxed oxide grains of about 200 nm in the outer side of the oxide and smaller grains ($\sim 50 \text{ nm}$) near the oxide/metal interface. Porosities are also remarked in the oxide scales, located mainly close to the oxide/metal interface. These porosities can favour cracking by weakening the mechanical resistance. Moreover, the different thermal expansion coefficients of oxide and metal lead to strong mechanical stresses at the oxide/metal interface during the cooling stage of the samples, after the oxidation process. The polishing process during the preparation of the samples can also propagate cracks at the oxide/metal interface. Such cracks can be observed between the oxide scale and the metal, for the S3 sample in Figure 2(f).

The metal shows large Ti grains in the lower part of the images and smaller grains at the oxide/metal interface, on the metal side. Such small grains have also been observed by Kitashima et al. [11] on a near alpha titanium alloy. The BSE mode revealed chemical contrast in the metal, near to the oxide/metal interface, suggesting that some grains close to the interface were enriched with lighter elements than oxygen, probably nitrogen. As shown previously by many authors, the metal is highly enriched in light elements, mainly oxygen, in the region close to the oxide/metal interface [1], [3–6,8–10],[22]. The small size

of the thin layers makes quantification of nitrogen near the oxide/metal interface hazardous by EDS techniques. This is one of the reasons why we will use further in the paper the NRA techniques to quantify the nitrogen concentration.

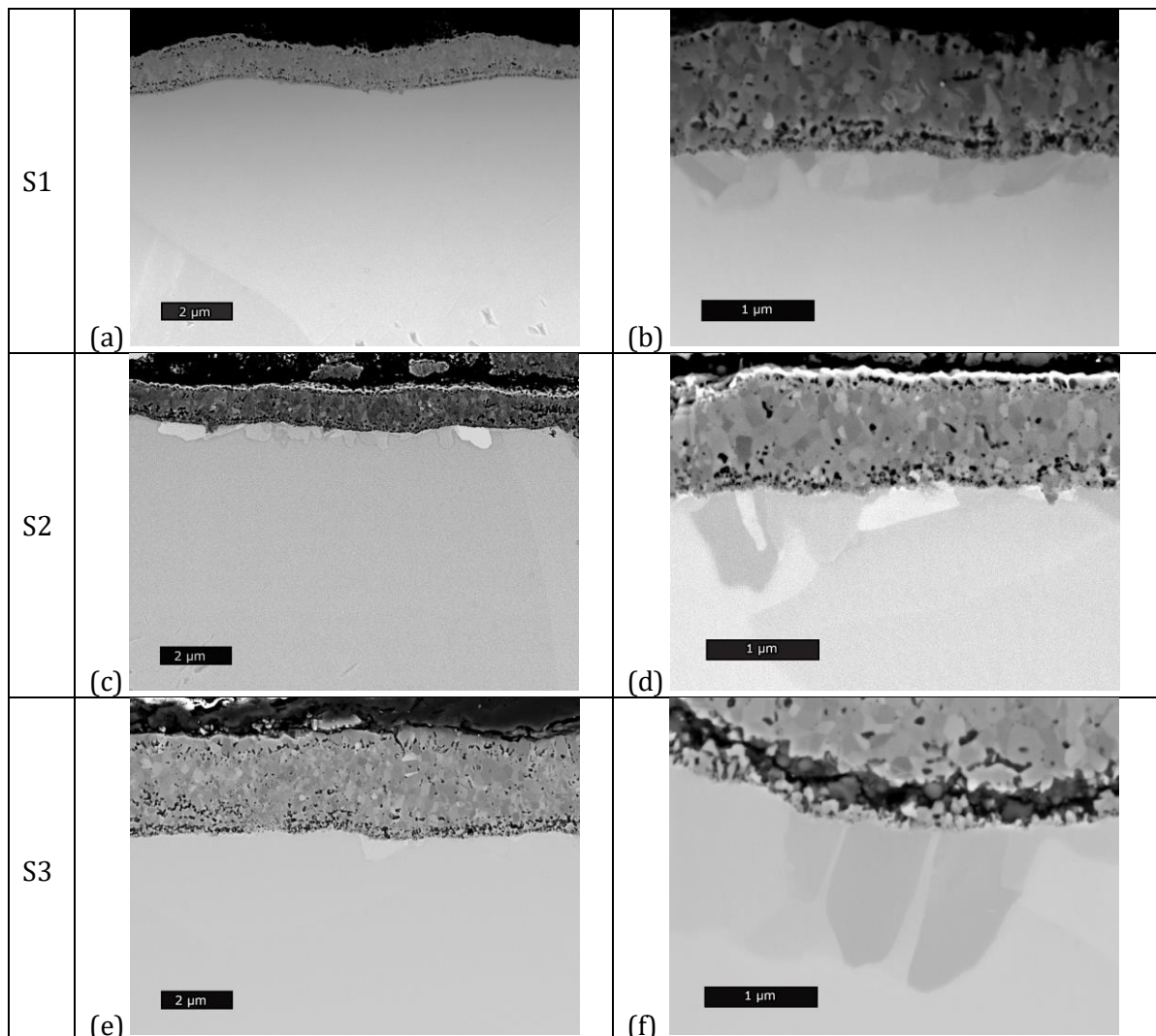


Figure 2. SEM images in back-scattered electrons mode (BSE). The oxide layer is located in the upper part of the images. The right column presents different spots, with higher magnification.

Elemental maps using EDS/WDS were made in order to reveal oxygen-rich and nitrogen-rich zones, as presented Figure 3. One can clearly see, as expected, the insertion of nitrogen at the interface. The Figure 3.(b), (d) and (e) show that the nitrogen accumulates at the top of the metal under the oxide/metal interface. Moreover, nitrogen seems to insert preferentially in some grains, while it is absent in others. It suggests that the nitrogen diffusion and insertion is probably an anisotropic process. It is worth to point out that the nitrogen-rich zone seems to form a discontinuous layer with thicknesses about $0.8 \mu\text{m}$ for S1 and S2 samples and $1.3 \mu\text{m}$ for S3. This feature has already been observed on pure Ti [3–5] or on titanium alloys [9]. WDS mappings confirm that in the nitrogen rich layers the oxygen is present in small quantities, which suggests that the oxygen must pass through the nitride layer to continue the diffusion within the metal. Small grains of nitrides have already been observed at the interface oxide/metal and were attributed to an oxidation-nitridation recrystallization, as already pointed out by Kitashima et al. [11].

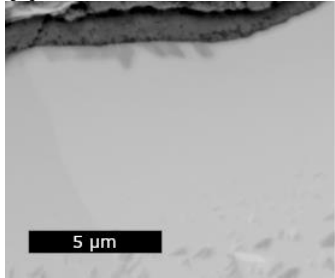
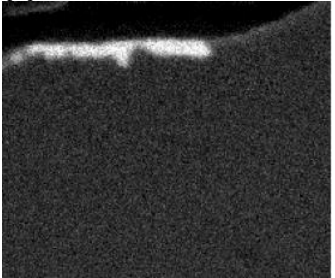
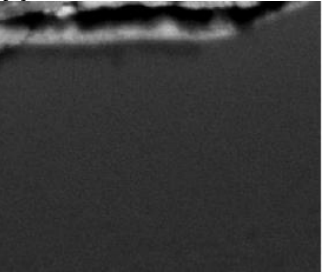
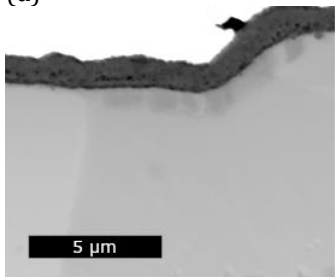
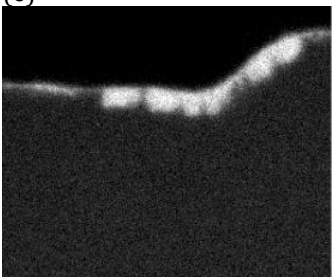
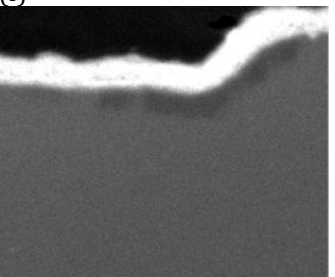
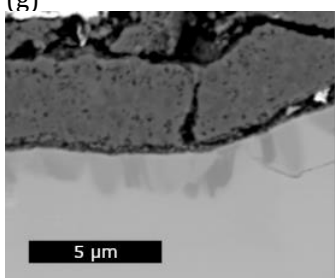
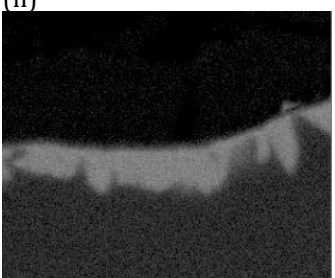
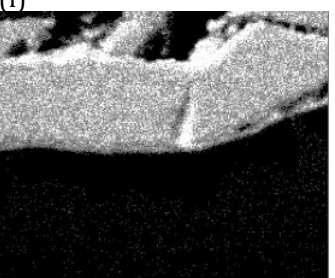
Sample	SEM image	Nitrogen (WDS)	Oxygen (EDS)
S1	(a) 	(b) 	(c) 
S2	(d) 	(e) 	(f) 
S3	(g) 	(h) 	(i) 

Figure 3. SEM images (BSE mode) and corresponding elemental cartographies (WDS for nitrogen and EDS for oxygen)

3.2.2. *Phases analysis*

The XRD patterns recorded in theta – theta mode are presented in Figure 4. As expected, the S1 and S2 samples show almost identical XRD patterns. The rutile TiO_2 and the alpha-titanium are the most visible phases. The relative intensity of the peaks of rutile with respect to alpha-Ti are clearly higher for the S3 sample compared to the S1 and S2 samples, as it was expected. The nitride phase $\text{Ti}_2\text{N}_{0.84}$ (tetragonal, ICDD 04-002-0574, which is an under-stoichiometric Ti_2N phase) is detected in all the patterns, but the peaks are barely visible because of the small quantity of this phase. This agrees with the presence of nitrogen detected by EDS/WDS (Figure 3), and with the results previously reported by Lavisse et al. [7] and Dupressoire et al. [8]. As expected, the S3 sample presents bigger rutile peaks.

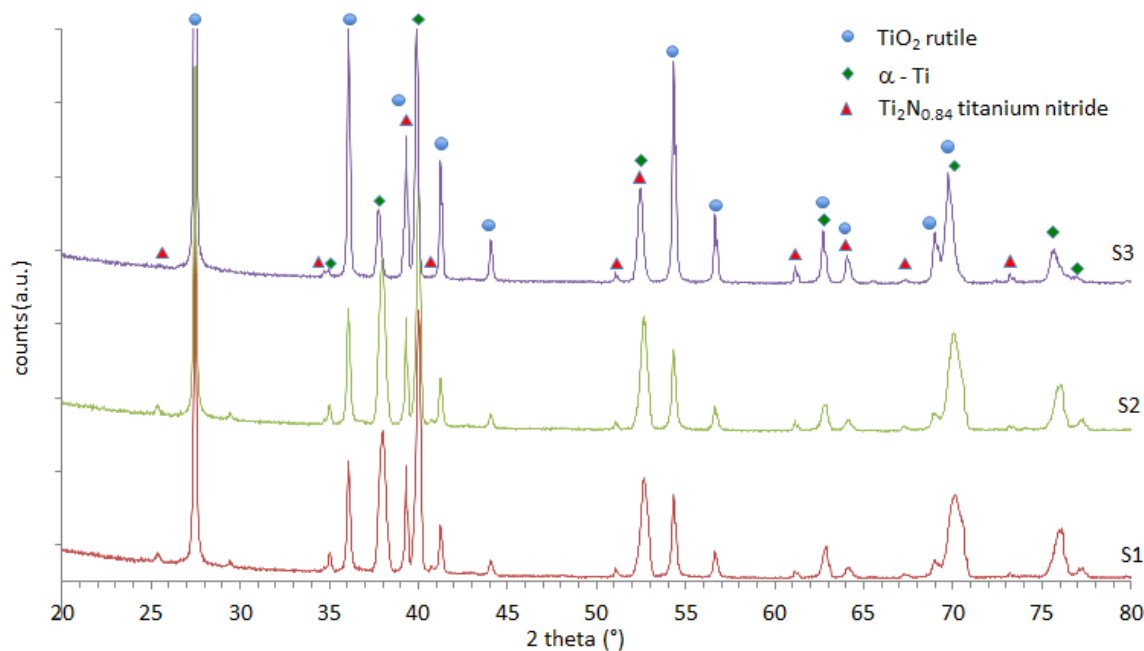


Figure 4. X-rays diffraction pattern (theta – theta mode) for the samples S1, S2 and S3.

Figure 5 shows the Raman spectra obtained for the samples S1, S2 and S3. The spectra were vertically shifted for clarity. All the spectra show the Raman bands of the rutile phase (marked as R on the graphic) of TiO_2 at 238 , 448 and 611 cm^{-1} [24]. In addition, a peak at 146 cm^{-1} clearly reveals the formation of TiO_2 crystallized in the anatase phase (marked as A on the graphic) for the 5h-oxidized samples, S1 and S2. The other Raman bands of the anatase phase at 399 , 514 and 639 cm^{-1} have a quite lower intensity and they are masked by the signal of the rutile phase. The intensity ratio between anatase and rutile bands slightly varies depending on the analysed area, but on average the spectra show the formation of a majority of rutile phase together with a small proportion of anatase phase. For the 20h-oxidized sample, S3, the intensity of the Raman peak at 146 cm^{-1} is very low compared to the rutile peaks. Moreover, the rutile phase also displays a very weak Raman mode of rutile at 143 cm^{-1} . All this indicates that the amount of anatase formed is negligible.

The spectra do not show, for any of the three samples, any feature, which can be assigned to oxynitride or nitride phases (TiN or Ti_2N). It is worth to remember that first order Raman scattering is forbidden in stoichiometric TiN due to the high O_h symmetry of its structure ($Fm\bar{3}m$). The presence of defects breaks the symmetry and allows to observe a weak Raman signal. This effect has been observed for example in titanium oxynitride thin films as a function of the N/O ratio [23]. Here, if present, the signal of TiN would be masked by that of the rutile phase. Concerning tetragonal Ti_2N , few works have analysed its Raman spectrum. Oghenevweta et al. [24] reported the spectra of nanocrystalline TiN and Ti_2N formed by ball milling of titanium powder under nitrogen atmosphere. Despite the low signal to noise ratio of the reported spectra, they assigned two bands at 340 and 456 cm^{-1} to nanocrystalline Ti_2N . In the spectra given in Figure 5, no band is observed at 340 cm^{-1} , and the strong signal of rutile at 448 cm^{-1} does not allow for the detection of other signals.

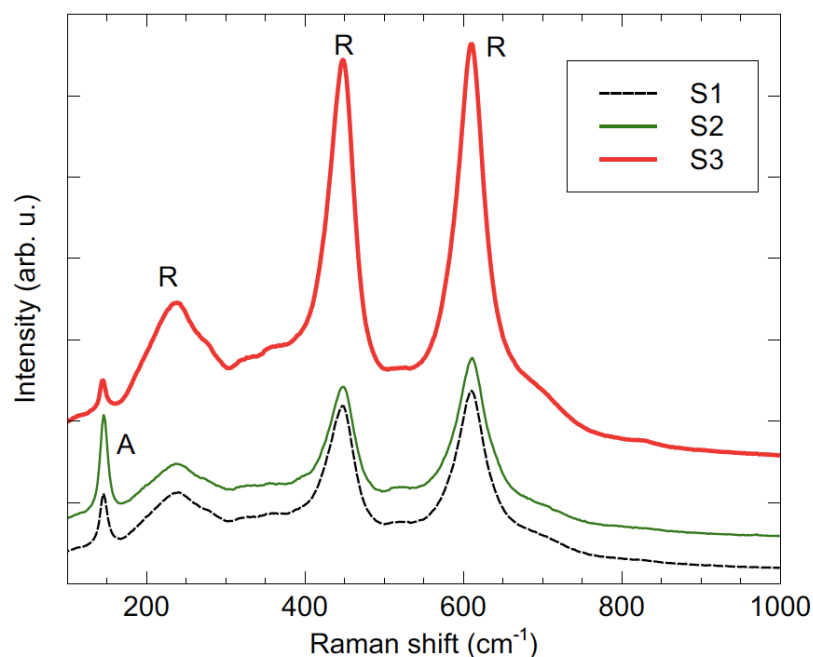


Figure 5. Raman spectra of the samples S1, S2 and S3.

Grazing incidence X-ray diffraction (GIXRD) was used for in-depth phase analysis of the oxidation layers in order to reveal the location of the nitride phase. The angles used here were 1°, 2°, 4°, 8°. The corresponding depths of penetration of X-rays in grazing incidence in rutile, at 90% of reflection of the X-Rays, were calculated using AbsorbDX software and are given in Table 4 for two values of 2θ angle.

Table 4. Penetration depth (in μm) of X-rays in TiO₂ rutile phase as a function of the incidence angle for detection angles 2θ equal to 30° and 60°.

	Incidence angle			
	1°	2°	4°	8°
2θ = 30°	0.7	1.4	2.6	4.4
2θ = 60°	0.7	1.5	2.8	5.2

The diffraction patterns in grazing mode for the sample S1 are shown in Figure 6 for several angles of incidence. The S2 sample shows almost identical diffraction patterns and thus will not be shown here. The identified phases were the rutile phase (tetragonal) of TiO₂, the alpha-Titanium (hexagonal close-packed) and the nitride close to the Ti₂N_{0.84} phase detected in Bragg-Bretano configuration, which is a Ti₂N-type nitride. One can notice several isolated peaks of nitride, oxide and metal, which permits to evaluate the maximum depth at which each layer is located. The nitride peaks are slightly perceptible at 1° of incidence angle, which suggests that the nitride phase is located deeper than 0.7 μm. They show a maximum of intensity at 4° of incidence, which indicates that most of the nitride phase must be above a depth of 2.8 μm. These results are in good agreement with those obtained by SEM/EDS/WDS analyses and they will be confirmed further in this article by NRA techniques.

The rutile peaks seem also to be maximum at 4° of incidence angle, which suggests that the oxide layer is entirely traversed by the X-rays at this angle. The alpha-titanium peaks

increase with the incidence angle, as expected. The very small peak observed at 43.05° can be assigned to oxynitrides of the family TiO_xN_y (such as $\text{TiO}_{0.78}\text{N}_{0.22}$ ICDD 04-001-9292, $\text{TiO}_{0.05}\text{N}_{0.58}$ ICDD 04-002-0428, $\text{TiO}_{0.78}\text{N}_{0.22}$ ICDD 04-002-0430 and $\text{TiO}_{0.14}\text{N}_{0.49}$ ICDD 04-002-0431) [25,26].

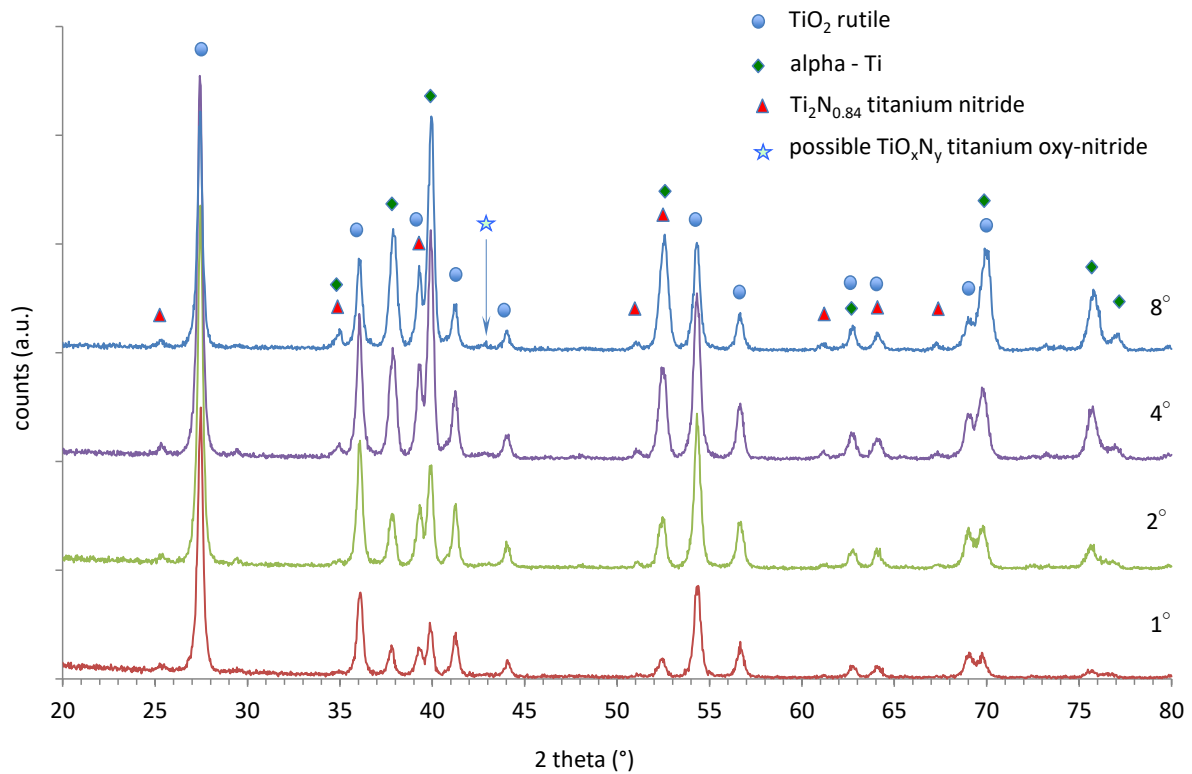


Figure 6. Grazing incidence X-rays diffraction pattern obtained for S1 sample (5h at 700°C under regular air) with different incidence angles.

The S3 sample's diffraction patterns presented in Figure 7 show the same phases as those detected for S1 (Figure 6). The notable difference is that no nitride can be detected at 1° and 2°, which according to Table 4 suggests that this phase is located deeper than 1.5 μm . The nitride peaks seem not to evolve between 4° and 8°, which suggests that the X-rays have probably passed through the entire nitride layer. The rutile peaks are smaller at 8° of incidence than at 4°, which shows that the oxide layer is entirely traversed at 4° of incidence. A small peak seems to be present at 43.3°, which can correspond to tiny quantities of titanium nitride TiN (face-centered cubic structure) or to TiO_xN_y phases cited above.

The Rietveld refinement technique was used to fit the GIXRD patterns of the samples S1, S2 and S3, in order to extract quantitative phase composition, lattice parameters and crystallite size. The quantitative phase composition must be taken as indicative, since the Rietveld refinement for layered structures is delicate. The results are given in Figure 8 and Figure A-1 in Appendix A. The S2 sample shows almost identical results (not shown here) to S1. Figure 8 displays the percentage of phase of rutile, titanium and titanium nitride phases. It shows that the proportion of rutile decreases by increasing the incidence angle, which means that the incident X-rays beam covered the entire thickness of the oxide layer for the smallest incidence angle. As expected, the alpha-titanium proportion is continuously growing with the incidence angle. The nitride proportion remains stable between 4° and 8°

of incidence for the S1 sample, which suggests that the entire nitride phase thickness was probed by the X-Rays.

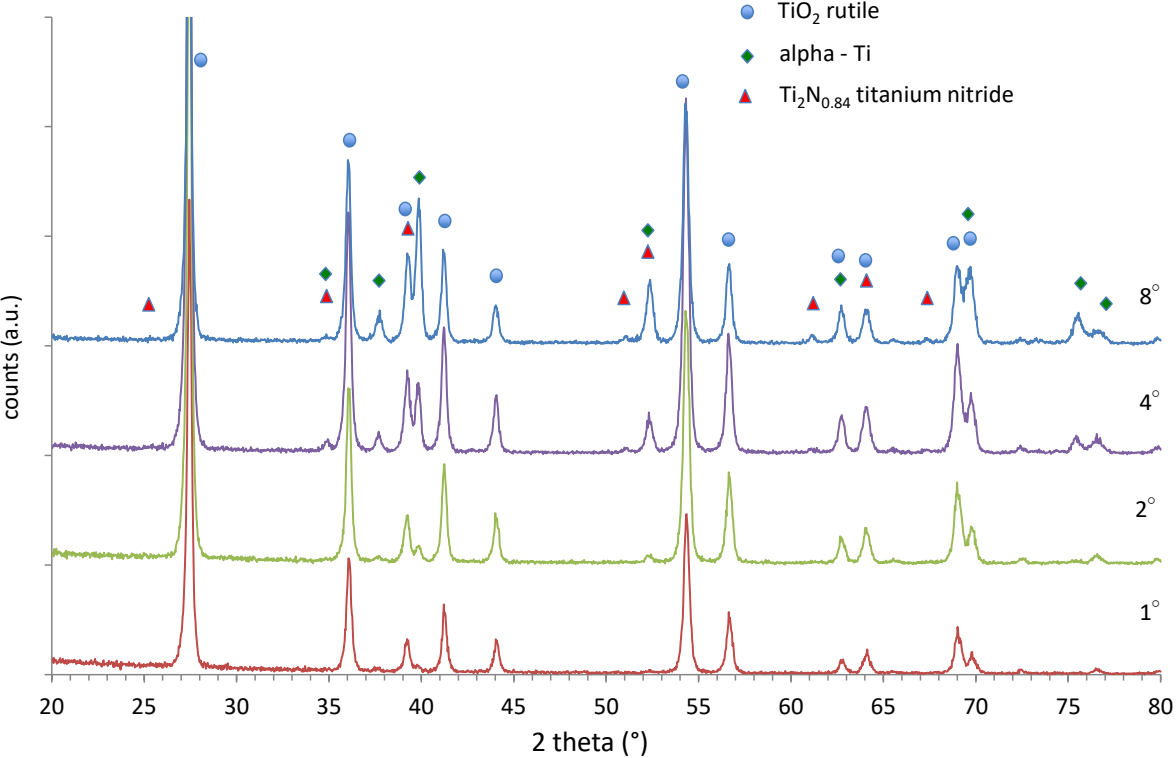


Figure 7. Grazing incidence X-rays diffraction pattern obtained for S3 sample (5h at 700 °C under ¹⁵N-labelled air followed by 15h under regular air) with different incidence angles.

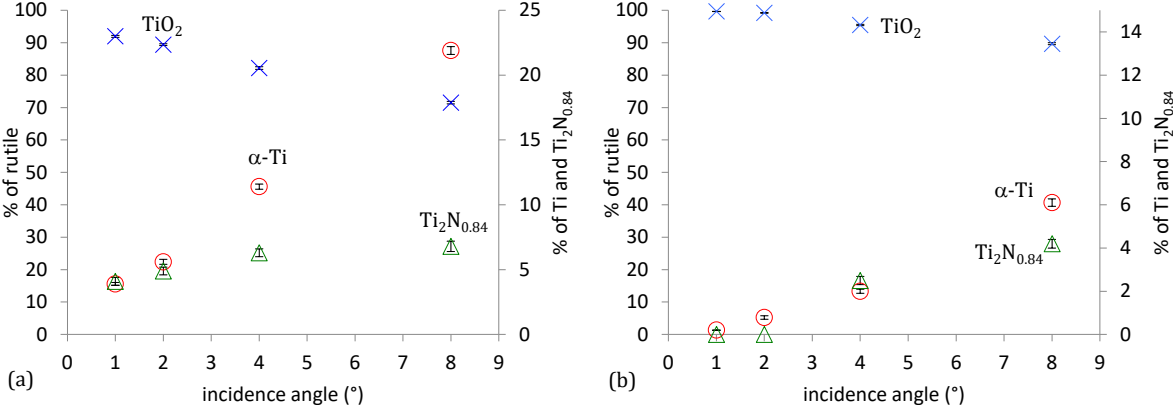


Figure 8. Percentage of the phases rutile, alpha-Ti and Ti₂N_{0.84} obtained by Rietveld refinement of the GIXRD patterns of: (a) S1 sample and (b) S3 sample, as a function of the incidence angle.

3.2.3. *In-depth analysis of the elemental distribution*

The Figure 9 presents the in-depth analyses by SIMS for the three samples over 40 x 40 μm². The profiles of the signals of ¹⁴N in S1 and ¹⁵N in S2 are very similar. They display a peak, which coincides with the decrease of the signal of ¹⁶O, which points out that the

nitrogen is located at the oxide/metal interface. This confirms the results obtained by XRD and agrees with the conclusions reported in refs [3–7] concerning the presence of a nitrogen-rich layer at this interface.

For the sample S3, the distribution of the isotope ^{14}N shows an intense and broad peak for a sputtering time of about 5500 seconds, and a weak bump at about 3200 seconds. The profile obtained for the isotope ^{15}N shows similar features, but the intensity of the main peak is quite lower, which agrees with the short exposition time of sample S3 to ^{15}N -labelled air compared to regular air. It is important to notice that the location of the both maximum pics of ^{14}N and ^{15}N in S3 sample are the same despite the fact that each isotope was introduced at different times within the sample. The peak of nitrogen concentration is correlated with a decrease in the oxygen signal, but the nitrogen seems to spread deeper than the oxygen. This agrees with SEM/EDS/WDS observations showing that nitrogen accumulates at the top of the metal, below the oxide/metal interface. The signal of nitrogen rises near the surface of the samples S1 and S2, while is wavy for S3 up to 4000s of sputtering time. The possibility of near-surface edge effects on this signal cannot be ruled-out. Further analysis is needed to confirm or not the presence of significant amount of nitrogen in the oxide scale. Moreover, the SIMS analysis does not allow to determine the amount of nitrogen inserted in the samples. Nuclear reaction analysis (NRA) is further used for this purpose.

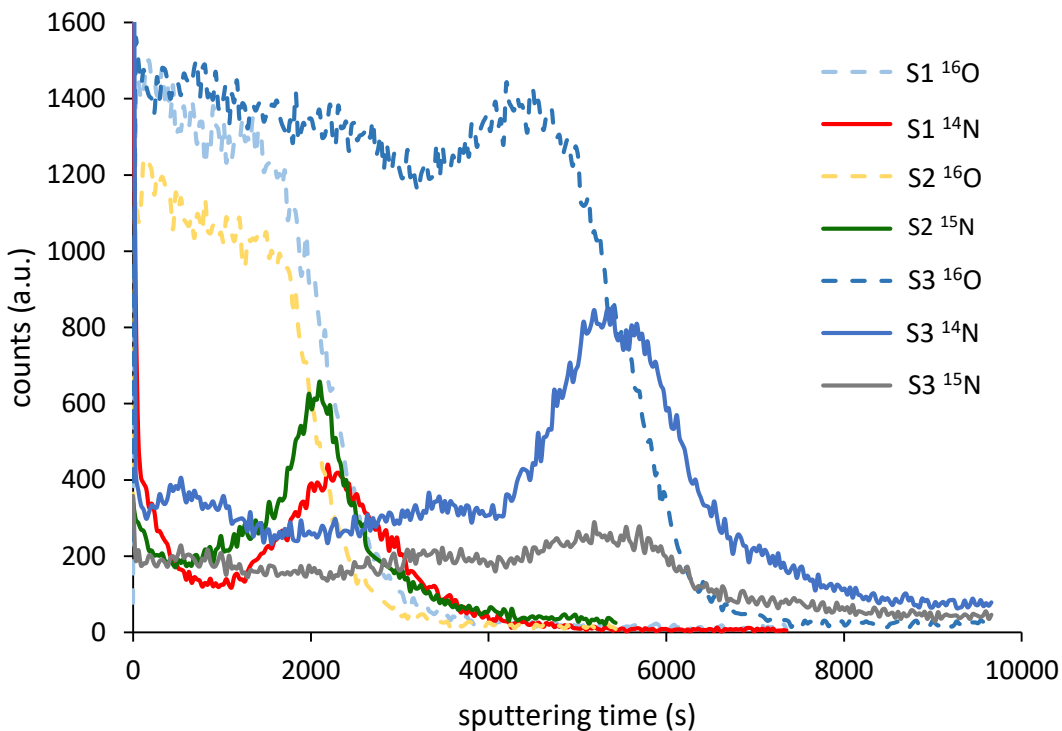


Figure 9. SIMS profile of the signals associated to the isotopes ^{16}O , ^{14}N and ^{15}N for the samples S1, S2 and S3 as a function of the sputtering time.

Figure 10 displays the NRA spectra of the samples S1, S2 and S3 in the range of [3.5 - 10 MeV]. They show several nuclear reactions induced on ^{14}N and ^{15}N isotopes; in particular,

the $^{14}\text{N}(d,\alpha_1)^{12}\text{C}$ and $^{15}\text{N}(d,\alpha_0)^{13}\text{C}$ reactions which have been used to determine the amount of ^{14}N , respectively ^{15}N isotopes inserted in the oxidized samples. Dashed vertical lines correspond to the energy of the different emitted particles when the reactions occur at the very surface of the sample (without any energy loss i.e. when no solid matter is crossed by the emitted particle). Their positions were calculated using the SIMNRA software [27] and confirmed by calibration samples. One can remark the shift of all the experimental peaks towards lower energies, which reflects the presence of ^{14}N and ^{15}N isotopes located under the oxide surface. The higher shift of the $^{14}\text{N}(d,\alpha_1)^{12}\text{C}$ reaction for the sample S3 compared to S1 shows that nitrogen is located deeper in the S3 sample. In the same way, the higher shift of the $^{15}\text{N}(d,\alpha_0)^{13}\text{C}$ reaction for the sample S3 compared to S2 shows that nitrogen is located deeper in S3.

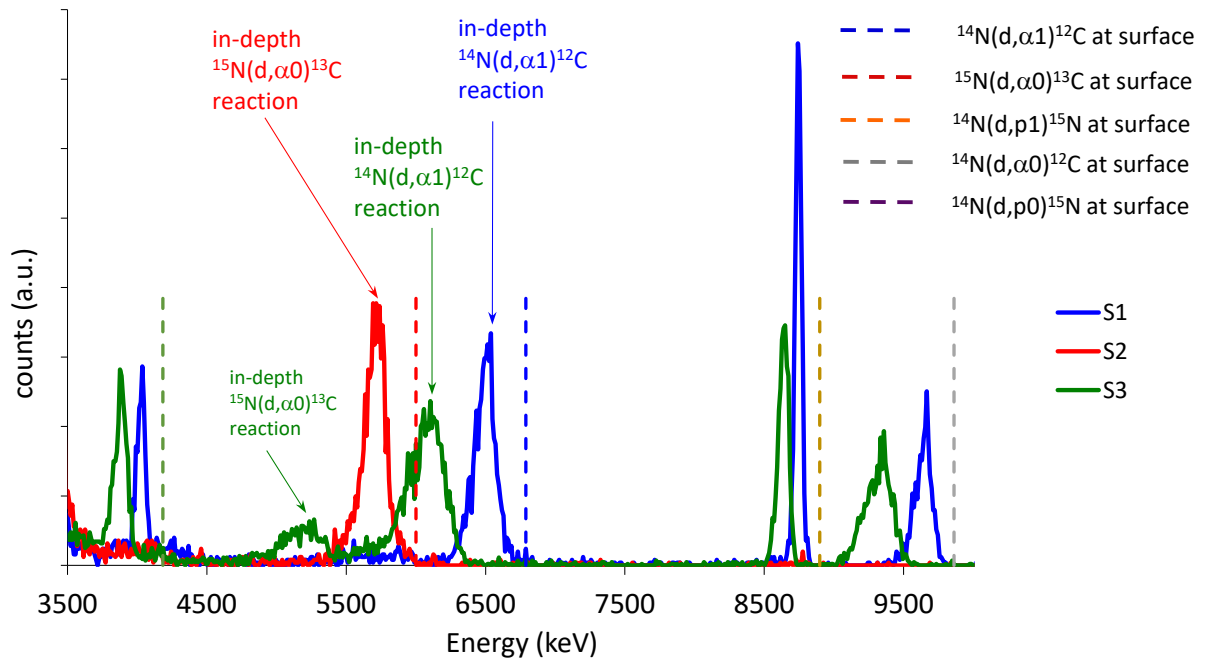


Figure 10. NRA spectra of S1, S2 and S3 samples showing the main nuclear reactions of ^{14}N and ^{15}N isotopes. The reactions $^{14}\text{N}(d,\alpha_1)^{12}\text{C}$ and $^{15}\text{N}(d,\alpha_0)^{13}\text{C}$ were used to determine the inserted amount of nitrogen. The calculated energies of the nuclear reactions produced at the extreme surface of the samples are drawn as reference.

In order to determine the in-depth distribution profiles of ^{14}N and ^{15}N isotope, we focused on the $^{14}\text{N}(d,\alpha_1)^{12}\text{C}$ and $^{15}\text{N}(d,\alpha_0)^{13}\text{C}$ reactions, respectively. This choice was driven by the fact that no other nuclear reactions interfere with these two reactions. The concentration of each isotope (^{14}N or ^{15}N) at a given depth was calculated using the intensity of the corresponding reaction in the NRA spectrum at a given energy and the cross-section of the reaction. The depth at which these reactions occur are obtained from the energy of the detected emitted particle. Figure 11 shows the profiles of nitrogen concentration obtained for S1, S2 and S3 samples obtained in this way, as a function of depth.

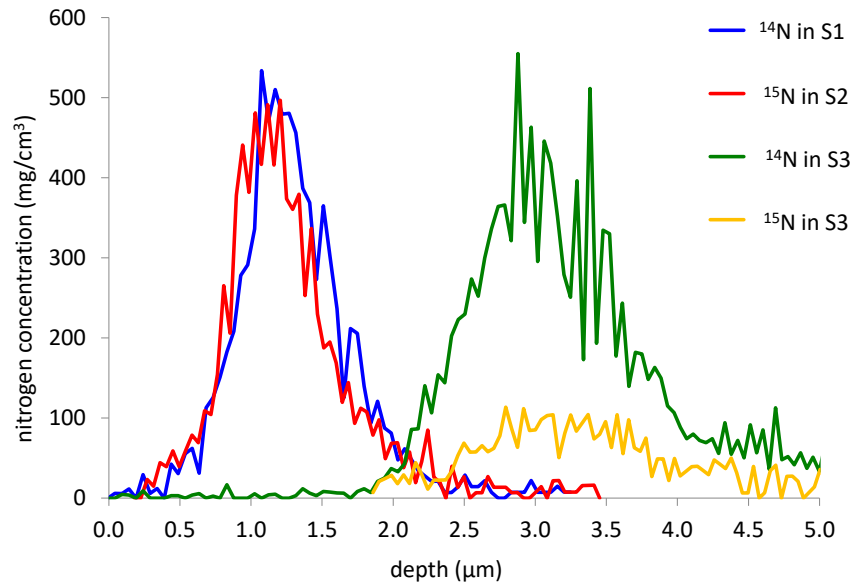


Figure 11. In-depth distribution of ^{14}N and ^{15}N isotopes in the samples S1, S2 and S3 after oxidation at 700°C .

As seen in Figure 11, the samples S1 and S2, which were oxidized for 5 h under regular air and ^{15}N -labeled air respectively, show very similar nitrogen insertions. Both samples present a maximum of nitrogen concentration at a depth of about $1.1\ \mu\text{m}$ under the sample surface. The thickness of the oxide layer observed by SEM/BSE was about $1\ \mu\text{m}$. The profiles of nitrogen obtained by NRA show the insertion of this element under the oxide/metal interface up to about $1.2\ \mu\text{m}$ in depth (based on TiO_2 density of $4.23\ \text{g}/\text{cm}^3$), which agrees with the WDS cartographies for nitrogen distribution in Figure 3. The profile of nitrogen obtained by NRA shows the presence of nitrogen above the oxide/metal interface. However, this result must be taken with care because the NRA analysis was done over a larger surface area ($200 \times 200\ \mu\text{m}^2$). As seen on the SEM/BSE images, the thicknesses of the various layers are not laterally homogeneous, which means that different phases, such as TiO_2 , Ti_2N , Ti-O solid solutions (and possibly TiN or oxynitrides) can be present at the same depth, each of them located in different regions.

The maximum concentration of nitrogen is about $500\ \text{mg}/\text{cm}^3$ in both the samples, which corresponds to a composition $\text{Ti}_2\text{N}_{0.76}$, if only Ti and N are considered. This composition is very close to that of the $\text{Ti}_2\text{N}_{0.84}$ phase detected by XRD.

As seen in Figure 11 for the S3 sample the two isotopes ^{14}N and ^{15}N are located at the same depth, which agrees also with the in-depth profiles obtained by SIMS for both isotopes (Figure 9). The maximum concentration of the two isotopes of nitrogen, ^{14}N and ^{15}N , is located at about $3\ \mu\text{m}$ in-depth, which corresponds to the average thickness of the oxide layer as seen on SEM/BSE views (Figure 3).

4. Discussion

4.1. In-depth distribution of nitrogen

In the previous section it has been shown (Figure 11) that both isotopes, ^{14}N and ^{15}N were located at the same depth within the sample S3. This result is surprising since the isotope

^{15}N was present only at the beginning of the oxidation up to 5 h, while the isotope ^{14}N was introduced later from 5 to 20 h. The diffusion coefficient of nitrogen in rutile is higher than that of oxygen [28]. So, the diffusion of nitrogen in the oxide scale is not the limiting step to its insertion in depth. On the contrary, the diffusion coefficient of nitrogen in metallic titanium is one order of magnitude smaller than that of oxygen [29–31]. Thus, the nitrogen can easily diffuse into the rutile and accumulates at the oxide/metal interface where it forms nitrides, as shown by XRD results. The WDS cartographies also show for the S3 sample the insertion of nitrogen in a discontinuous layer about $1.3\ \mu\text{m}$ thick on the top of the metal. The nitrogen concentration profile obtained by NRA are slightly broader. However (as argued for the samples S1 and S2), the inhomogeneity in thickness of the oxide and nitride layers induces a broadening of the nitrogen distribution profile, and can explain the detection of some amount of nitrogen up to about $1\ \mu\text{m}$ above the oxide/metal interface. Our results differ from those reported by Göbel et al. [14] who studied by secondary neutral mass spectroscopy the insertion of isotope-labelled oxygen and nitrogen in pure Ti and Ti-4Nb in two-stages oxidation experiments during 5 hours at $800\ ^\circ\text{C}$ in a humid atmosphere. They found that the nitrogen used in the first stage of oxidation diffused deeper into the material than that used in the second stage. They concluded that in pure Ti the dissolution of nitrogen in the substrate at the nitride/substrate interface dominates over the formation of new nitride at the oxide/nitride interface. Our study provides different results using both NRA and SIMS techniques, showing that the nitrogen used in both stages of oxidation is located at the same position. It is worth to mention that in our case the oxidation experiments were done in dry air at a lower temperature (700°C) and for longer oxidation times.

Another interesting fact is that the maximum concentration of nitrogen detected by NRA does not seem to depend on the exposure time, which suggests that the same nitride compound is generated, probably an under-stoichiometric Ti_2N , as revealed by the XRD. It should be noted that the bell-shape nitrogen profile broadens with the oxidation time. Thus, the overall amount of nitrogen increases with the exposure time.

4.2 Nitrogen mass gain during oxidation

By integrating the profiles of nitrogen concentration over the depth obtained by NRA (Figure 11), one can obtain the nitrogen mass gain per unit area given in Table 5.

For the samples oxidized 5 h, S1 and S2, the nitrogen (^{14}N and ^{15}N , respectively) mass gain values are almost the same, about $40\ \mu\text{g}/\text{cm}^2$. For the sample S3 the amount of ^{15}N inserted after 5 h of exposure drops down to $28\ \mu\text{g}/\text{cm}^2$ after 15 h of supplementary oxidation under regular air. At the same time $57\ \mu\text{g}/\text{cm}^2$ of ^{14}N are inserted during the 15 h second oxidation stage. The partial replacement of ^{15}N inserted in the first oxidation stage by ^{14}N in the second oxidation stage shows that nitrogen does not have only a one-way diffusion direction downward in the metal, but it can also desorb from the sample to return to the atmosphere. There is a permanent flow of nitrogen inward and outward the sample promoted by the thermal agitation at high temperature. This answers to the third question raised in the Introduction section, and shows that there is a partial renewal of the nitrogen during the high temperature oxidation of titanium.

The XRD analysis showed the formation of a nitride phase close to Ti_2N at the oxide/metal interface. Assuming that all the inserted nitrogen is in the form of Ti_2N , one can calculate

the thickness of a layer of a Ti₂N equivalent to the amount of the measured nitrogen mass gain. The values given in Table 5 vary from around 0.6 μm for the samples S1 and S2 to around 1.3 μm for the sample S3. These values are in good agreement with those observed on SEM/BSE images and WDS cartographies (Figure 3). This shows that most of the inserted nitrogen is part of the nitrides formed at the oxide/metal interface. Moreover, this represents also an independent validation of the amounts of nitrogen obtained by NRA.

The total amount of nitrogen roughly doubles from 5 to 20 h of exposure to high temperature. This suggests that the nitrogen mass gain could increase according to a parabolic law, but further measurements for different oxidation durations are still needed to validate this assertion.

The nitrogen mass gained during the exposure to high temperature represents a small percentage of the total mass gain measured by weighing. The values obtained for the samples S1, S2 and S3 are given in Table 5. The percentage of nitrogen in the total mass gain is about 16 % for the samples oxidized during 5h and decreases to about 12 % for the sample S3 after 20 h of exposure to high temperature.

Table 5. Nitrogen and total mass gain per unit area obtained for the samples S1, S2 and S3. The nitrogen mass gain was determined by NRA analysis. The thickness of an equivalent Ti₂N layer was calculated by assuming a density of 4.88 g/cm³. The total mass gain was obtained by weighing.

Sample	Isotope	Exposure time (h)	Nitrogen mass gain (μg/cm ²)	Thickness of equivalent Ti ₂ N layer (μm)	Total mass gain (μg/cm ²)	Percentage of Nitrogen in the total mass gain (%)
S1	¹⁴ N	5	41	0.66	251	16.3
S2	¹⁵ N	5	39	0.59	245	15.5
S3	¹⁵ N	5	28			
S3	¹⁴ N	15	57			
S3	¹⁴ N & ¹⁵ N	5+15	85	1.34	689	12.3

4.3 Cycle of life of nitrides during the high temperature oxidation of titanium in air

The results presented above lead us to propose the following model (graphically summarized in Figure 12) for the evolution of the inserted nitrogen during the high temperature oxidation of titanium.

The nitrides formed at the oxide/metal interface are a slowing diffusion barrier for the oxygen coming by anionic diffusion through the oxide. The nitrides barrier produces the drop of the oxygen partial pressure under the nitrides (at the nitrides/metal interface) and simultaneously the rise of the oxygen partial pressure above the oxide/nitrides interface. This rise of the oxygen partial pressure produces the oxidation of the upper part of the nitrides, and the release of nitrogen. Part of this nitrogen can diffuse on short distances into the metal (to occupy the sites freed by the oxygen that diffused further to the core of the material) and form new nitrides. This produces a migration of nitrides in the direction of

the metal. The rest of the nitrogen liberated by the oxidation of the nitrides can diffuse through the oxide scale and partially desorb at the surface of the oxide layer. At the same time, atmospheric nitrogen continues to diffuse inward and participate to the formation of new nitrides. The result is a progression of the nitrides to the core of the material at the same time as the oxide scale thickness grows. Thus, the kinetics of nitrogen insertion is limited by the formation of the nitrides at the oxide/metal interface and their oxidation by the inward flow of oxygen.

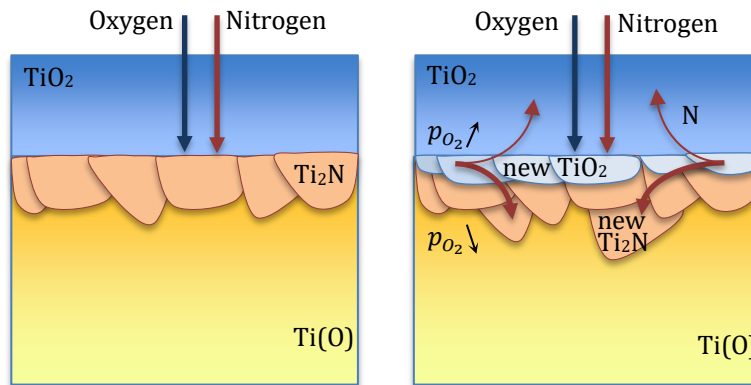


Figure 12. Cycle of life of nitrides during the oxidation in air at 700°C.

5. Conclusion

The insertion of nitrogen during the high temperature oxidation of pure titanium was studied by two-steps oxidation experiments using regular air and in ^{15}N -labelled air for durations of 5 and 20 h at 700 °C. The main goal was to determine, for the first time to our knowledge, the amount of nitrogen inserted at the oxide/metal interface and to analyse its variation during the exposure at 700 °C. For this purpose, several techniques were used to analyse the samples oxidized in regular and ^{15}N -labelled air (SEM, EDS/WDS, XRD, Raman, SIMS). In particular, Nuclear Reaction Analysis was used to quantify the insertion of nitrogen.

Our results confirm that the nitrogen locates at the oxide/metal interface from the very beginning of the exposure of titanium to high temperature, as reported in previous works. In addition, the following conclusions can be drawn regarding the stated objectives of this work:

- The inserted nitrogen forms a distinctive nitride phase, identified by XRD as an under-stoichiometric Ti_2N phase (namely $\text{Ti}_2\text{N}_{0.84}$). It forms a discontinuous layer located on top of the metal, under the oxide scale, as shown by WDS cartographies.
- The nitrogen is localized at the interface oxide/metal and its diffusion deeper into the metal seems negligible according to the analyses by SIMS and NRA.
- The nitrogen mass gain was evaluated from NRA results to $40 \mu\text{g}/\text{cm}^2$ for 5h of exposure at 700°C, which corresponds to around 16 % of the total mass gain.
- The amount of inserted nitrogen was almost doubled for 20 hours of exposure, which suggests a parabolic-like nitrogen mass gain. Around 12.5 % of the total mass gain corresponds to the nitrogen while the oxygen represents the remaining 77.5 %.
- The limiting step of the nitrogen insertion during the oxidation of titanium in air seems to be the formation of nitrides at the oxide/metal interface and their

oxidation. The presence of these nitrides acts as a slowing barrier for oxygen penetration into the metal.

- A model for nitrides migration is proposed

Credit authorship contribution statement

V. Optasanu: Conceptualization, Methodology, Experimental setup, Investigation, Validation, Formal analysis, Data curation, Visualization, Writing - review & editing, Project administration, P. Berger: Investigation, Methodology, Formal analysis, Writing - review. M. Khan Rayan: Experimental Setup, Resources, Investigation. F. Herbst: Investigation. N. Geoffroy: Investigation. M.C. Marco de Lucas: Investigation, Validation, Writing – review. O. Heintz: Investigation, S. Chevalier: Experimental setup. I. Bezverkhy: Experimental setup, Validation. T. Montesin: Validation, project administration. L. Lavis: Conceptualization, Validation, Formal analysis, Writing – review.

Data availability statement

The raw/processed data required to reproduce these findings cannot be shared at this time as the data also forms part of an ongoing study.

Conflict of interest

The authors declare that they have no known competing financial interests or personal relationships that could have appeared to influence the work reported in this paper.

Acknowledgements

The authors thank to Prof. J.-P. Bellat for his expertise in the conception of the nitrogen trapping system. This work was supported by the EIPHI Graduate School (contract ANR-17-EURE-0002).

References

- [1] P. Kofstad, *High Temperature Corrosion*, Elsevier Applied Science, 1988.
- [2] A.M. Chaze, C. Coddet, The role of nitrogen in the oxidation behaviour of titanium and some binary alloys, *J. Common Met.* 124 (1986) 73–84.
[https://doi.org/10.1016/0022-5088\(86\)90478-9](https://doi.org/10.1016/0022-5088(86)90478-9).
- [3] A. Kanjer, V. Optasanu, L. Lavissee, M. del C.M. de Lucas, S. Dejardin, M. François, P. Berger, P. Peyre, C. Gorny, T. Montesin, Influence of mechanical surface treatment on high-temperature oxidation of pure titanium, *Oxid. Met.* 88 (2017) 383–395.
- [4] A. Kanjer, L. Lavissee, V. Optasanu, P. Berger, C. Gorny, P. Peyre, F. Herbst, O. Heintz, N. Geoffroy, T. Montesin, M.C. Marco de Lucas, Effect of laser shock peening on the high temperature oxidation resistance of titanium, *Surf. Coat. Technol.* 326 (2017) 146–155. <https://doi.org/10.1016/j.surfcoat.2017.07.042>.
- [5] A. Kanjer, V. Optasanu, M.C. Marco de Lucas, O. Heintz, N. Geoffroy, M. François, P. Berger, T. Montesin, L. Lavissee, Improving the high temperature oxidation resistance of pure titanium by shot-peening treatments, *Surf. Coat. Technol.* 343 (2018) 93–100. <https://doi.org/10.1016/j.surfcoat.2017.10.065>.
- [6] L. Lavissee, A. Kanjer, P. Berger, V. Optasanu, C. Gorny, P. Peyre, T. Montesin, M.C. Marco de Lucas, High temperature oxidation resistance and microstructure of laser-shock peened Ti-Beta-21S, *Surf. Coat. Technol.* 403 (2020) 126368.
<https://doi.org/10.1016/j.surfcoat.2020.126368>.
- [7] L. Lavissee, P. Berger, A. Kanjer, V. Optasanu, C. Gorny, P. Peyre, M. François, T. Montesin, M.C. Marco de Lucas, Tracking the role of nitrogen in the improvement of the high temperature oxidation resistance of titanium by mechanical treatments, *Corros. Sci.* 197 (2022) 110080. <https://doi.org/10.1016/j.corsci.2021.110080>.
- [8] C. Dupressoire, A. Rouaix-Vande Put, P. Emile, C. Archambeau-Mirguet, R. Peraldi, D. Monceau, Effect of Nitrogen on the Kinetics of Oxide Scale Growth and of Oxygen Dissolution in the Ti6242S Titanium-Based Alloy, *Oxid. Met.* 87 (2017) 343–353.
<https://doi.org/10.1007/s11085-017-9729-1>.
- [9] I. Abdallah, C. Dupressoire, L. Laffont, D. Monceau, A. Vande Put, STEM-EELS identification of TiOXNY, TiN, Ti₂N and O, N dissolution in the Ti₂642S alloy oxidized in synthetic air at 650 °C, *Corros. Sci.* 153 (2019) 191–199.
<https://doi.org/10.1016/j.corsci.2019.03.037>.
- [10] C. Dupressoire, M. Descoins, A.V. Put, E. Epifano, D. Mangelinck, P. Emile, D. Monceau, The role of nitrogen in the oxidation behaviour of a Ti₂642S alloy: a nanoscale investigation by atom probe tomography, *Acta Mater.* (2021) 117134.
<https://doi.org/10.1016/j.actamat.2021.117134>.
- [11] T. Kitashima, T. Hara, Y. Yang, Y. Hara, Oxidation–nitridation-induced recrystallization in a near- α titanium alloy, *Mater. Des.* 137 (2018) 355–360.
<https://doi.org/10.1016/j.matdes.2017.10.043>.
- [12] V.A.C. Haanappel, J.D. Sunderkötter, M.F. Stroosnijder, The isothermal and cyclic high temperature oxidation behaviour of Ti–48Al–2Mn–2Nb compared with Ti–48Al–2Cr–2Nb and Ti–48Al–2Cr, *Intermetallics.* 7 (1999) 529–541.
[https://doi.org/10.1016/S0966-9795\(98\)00076-4](https://doi.org/10.1016/S0966-9795(98)00076-4).
- [13] E. Carpenne, M. Shinn, P. Schaaf, Free-electron laser surface processing of titanium in nitrogen atmosphere, *Appl. Surf. Sci.* 247 (2005) 307–312.
<https://doi.org/10.1016/j.apsusc.2005.01.059>.
- [14] M. Göbel, J.D. Sunderkötter, D.I. Mircea, H. Jenett, M.F. Stroosnijder, Study of the high-temperature oxidation behaviour of Ti and Ti₄Nb with SNMS using tracers, *Surf.*

- Interface Anal. 29 (2000) 321–324. [https://doi.org/10.1002/\(SICI\)1096-9918\(200005\)29:5<321::AID-SIA872>3.0.CO;2-Q](https://doi.org/10.1002/(SICI)1096-9918(200005)29:5<321::AID-SIA872>3.0.CO;2-Q).
- [15] P. Trocellier, P. Berger, M. Wilde, Nuclear Reaction Analysis, in: *Encycl. Anal. Chem.*, John Wiley & Sons, Ltd, 2016: pp. 1–17. <https://doi.org/10.1002/9780470027318.a6208.pub3>.
- [16] M. Peisach, Nuclear Reaction Analysis, in: *Elem. Anal. Part. Accel.*, CRC Press, 1992.
- [17] Agence internationale de l'énergie atomique, Ion beam techniques for the analysis of light elements in thin films, including depth profiling: final report of a co-ordinated research project 2000-2003., International Atomic Energy Agency, Vienna, 2004. http://www-pub.iaea.org/MTCD/publications/PDF/te_1409_web.pdf (accessed November 30, 2021).
- [18] H. Khodja, E. Berthoumieux, L. Daudin, J.-P. Gallien, The Pierre Süe Laboratory nuclear microprobe as a multi-disciplinary analysis tool, *Nucl. Instrum. Methods Phys. Res. Sect. B Beam Interact. Mater. At.* 181 (2001) 83–86. [https://doi.org/10.1016/S0168-583X\(01\)00564-X](https://doi.org/10.1016/S0168-583X(01)00564-X).
- [19] Ion Beam Analysis Nuclear Data Library (IBANDL), (n.d.). <https://www-nds.iaea.org/exfor/ibandl.htm> (accessed February 13, 2022).
- [20] M. Kokkoris, X. Aslanoglou, M. Axiotis, A. Lagoyannis, K. Michalakis, P. Misaelides, E. Ntemou, N. Patronis, K. Preketes-Sigalas, P. Tsintari, Study of differential cross-sections of the $^{14}\text{N}(d,\alpha)^{13}\text{C}$ reactions suitable for NRA, *Nucl. Instrum. Methods Phys. Res. Sect. B Beam Interact. Mater. At.* 450 (2019) 31–36. <https://doi.org/10.1016/j.nimb.2018.08.034>.
- [21] I.C. Vickridge, W.J. Trompeter, G.E. Coote, $^{15}\text{N}(d,\alpha)^{13}\text{C}$ cross section and angular distribution measurements for ion beam analysis, *Nucl. Instrum. Methods Phys. Res. Sect. B Beam Interact. Mater. At.* 108 (1996) 367–370. [https://doi.org/10.1016/0168-583X\(95\)01165-X](https://doi.org/10.1016/0168-583X(95)01165-X).
- [22] M. Berthaud, I. Popa, R. Chassagnon, O. Heintz, J. Lavková, S. Chevalier, Study of titanium alloy Ti6242S oxidation behaviour in air at 560°C: Effect of oxygen dissolution on lattice parameters, *Corros. Sci.* 164 (2020) 108049. <https://doi.org/10.1016/j.corsci.2019.06.004>.
- [23] A. Trenczek-Zajac, M. Radecka, K. Zakrzewska, A. Brudnik, E. Kusior, S. Bourgeois, M.C.M. de Lucas, L. Imhoff, Structural and electrical properties of magnetron sputtered Ti(ON) thin films: The case of TiN doped in situ with oxygen, *J. Power Sources.* 194 (2009) 93–103. <https://doi.org/10.1016/j.jpowsour.2008.12.112>.
- [24] J.E. Oghenevweta, D. Wexler, A. Calka, Understanding reaction sequences and mechanisms during synthesis of nanocrystalline Ti₂N and TiN via magnetically controlled ball milling of Ti in nitrogen, *J. Mater. Sci.* 53 (2018) 3064–3077. <https://doi.org/10.1007/s10853-017-1734-x>.
- [25] D. Dolat, D. Moszyński, N. Guskos, B. Ohtani, A.W. Morawski, Preparation of photoactive nitrogen-doped rutile, *Appl. Surf. Sci.* 266 (2013) 410–419. <https://doi.org/10.1016/j.apsusc.2012.12.048>.
- [26] A.J. Antończak, Ł. Skowroński, M. Trzcinski, V.V. Kinzhybalo, Ł.K. Łazarek, K.M. Abramski, Laser-induced oxidation of titanium substrate: Analysis of the physicochemical structure of the surface and sub-surface layers, *Appl. Surf. Sci.* 325 (2015) 217–226. <https://doi.org/10.1016/j.apsusc.2014.11.062>.
- [27] M. Mayer, Improved physics in SIMNRA 7, *Nucl. Instrum. Methods Phys. Res. Sect. B Beam Interact. Mater. At.* 332 (2014) 176–180.
- [28] M. Raffy, Thèse de doctorat, Ecole Nationale Supérieure de Chimie de Paris, 1981.
- [29] H. Nakajima, M. Koiwa, Diffusion in titanium, *ISIJ Int.* 31 (1991) 757–766.

- [30] A. Anttila, J. Räsänen, J. Keinonen, Diffusion of nitrogen in α -Ti, *Appl. Phys. Lett.* 42 (1983) 498–500. <https://doi.org/10.1063/1.93981>.
- [31] D. David, A Study of the Diffusion of Oxygen in α -Titanium Oxidized in the Temperature Range 460°–700°C, *J. Electrochem. Soc.* 130 (1983) 1423. <https://doi.org/10.1149/1.2119966>.

List of Figure captions:

Figure 1. Experimental device for isotopic labelling during oxidation.

Figure 2. SEM images in back-scattered electrons mode (BSE). The oxide layer is located in the upper part of the images.

Figure 3. SEM images (BSE mode) and corresponding elemental cartographies (WDS for nitrogen and EDS for oxygen)

Figure 4. X-rays diffraction pattern (theta – theta mode) for the samples S1, S2 and S3.

Figure 5. Raman spectra of the samples S1, S2 and S3.

Figure 6. Grazing incidence X-rays diffraction pattern obtained for S1 sample (5h at 700°C under regular air) with different incidence angles.

Figure 7. Grazing incidence X-rays diffraction pattern obtained for S3 sample (5h at 700 °C under 15N-labelled air followed by 15h under regular air) with different incidence angles.

Figure 8. Percentage of the phases rutile, alpha-Ti and Ti₂N_{0.84} obtained by Rietveld refinement of the GIXRD patterns of: (a) S1 sample and (b) S3 sample, as a function of the incidence angle.

Figure 9. SIMS profile of the signals associated to the isotopes ¹⁶O, ¹⁴N and ¹⁵N for the samples S1, S2 and S3 as a function of the sputtering time.

Figure 10. NRA spectra of S1, S2 and S3 samples showing the main nuclear reactions of ¹⁴N and ¹⁵N isotopes. The reactions ¹⁴N(d,α¹)¹²X and ¹⁵N(d,α⁰)¹³X were used to determine the inserted amount of nitrogen. The calculated energies of the nuclear reactions produced at the extreme surface of the samples are drawn as reference.

Figure 11. In-depth distribution of ¹⁴N and ¹⁵N isotopes in the samples S1, S2 and S3 after oxidation at 700°C.

Figure 12. Cycle of life of nitrides during the oxidation in air at 700°C.

Figure A-13. Variation of the lattice parameters as a function of the incidence angle in GIXRD patterns: (a) S1 rutile, (b) S1 α-Ti, (c) S3 rutile, (d) S3 α-Ti.

List of the Tables caption:

Table 1. Ti samples identification and corresponding oxidation treatments.

Table 2. Experimental conditions of the Nuclear Reaction Analysis used for this experiment and nuclear reactions used to reveal the nitrogen isotopes.

Table 3. Measured mass gain per unit area of the samples after various expositions at 700°C.

Table 4. Penetration depth (in μm) of X-rays in TiO_2 rutile phase as a function of the incidence angle for detection angles 2θ equal to 30° and 60°

Table 5. Nitrogen and total mass gain per unit area obtained for the samples S1, S2 and S3. The nitrogen mass gain was determined by NRA analysis. The thickness of an equivalent Ti_2N layer was calculated by assuming a density of 4.88 g/cm^3 . The total mass gain was obtained by weighing.

Appendix A

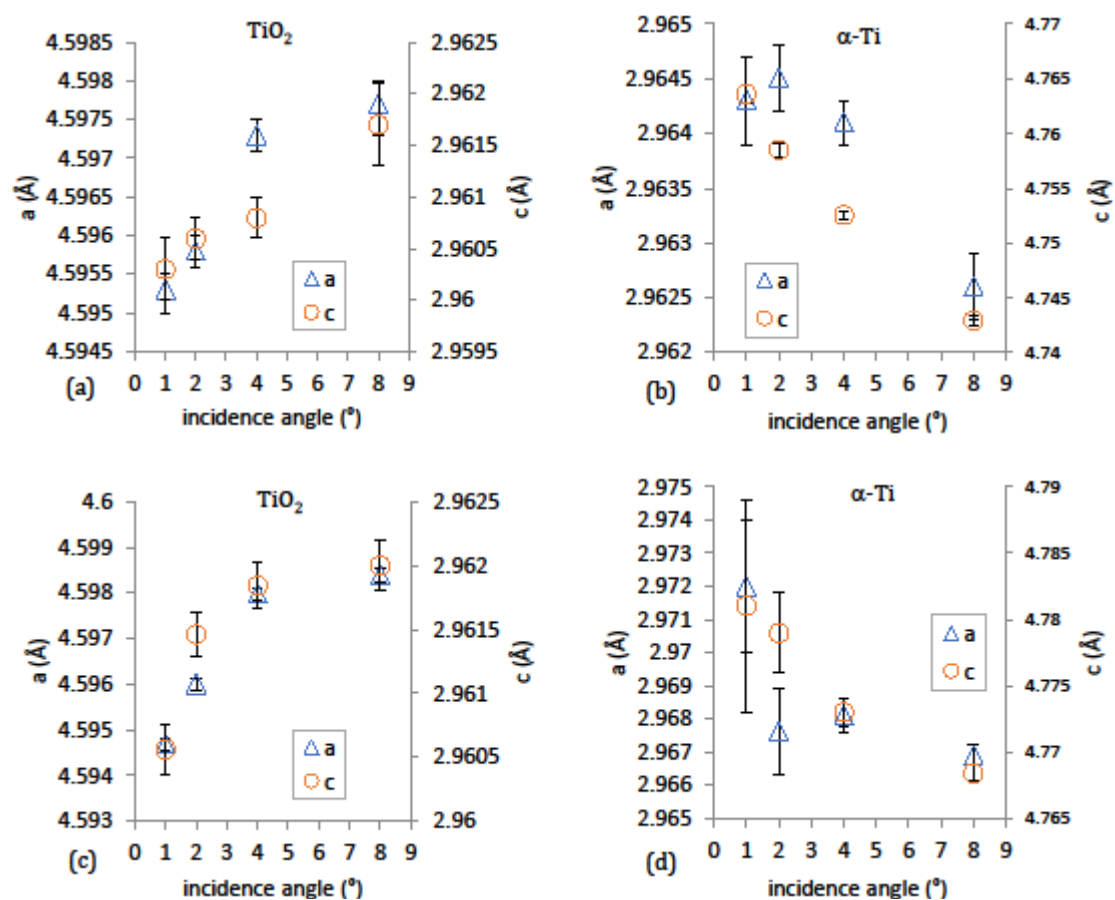


Figure A-13. Variation of the lattice parameters as a function of the incidence angle in GIXRD patterns: (a) S1 rutile, (b) S1 $\alpha\text{-Ti}$, (c) S3 rutile, (d) S3 $\alpha\text{-Ti}$.